



AD-A212 674

**Evaluation of the Near-Wall  $k-\epsilon$  Turbulence  
Model by Comparison with Direct Simulations of  
Turbulent Channel Flow**

E. WADE MINER, THOMAS F. SWEAN, JR.,  
ROBERT A. HANDLER AND RICHARD I. LEIGHTON

*Center for Fluid Dynamic Developments  
Laboratory for Computational Physics and Fluid Dynamics*

September 7, 1989



## REPORT DOCUMENTATION PAGE

Form Approved  
OMB No 0704-0188

1a REPORT SECURITY CLASSIFICATION <b>UNCLASSIFIED</b>			1b RESTRICTIVE MARKINGS		
2a SECURITY CLASSIFICATION AUTHORITY			3 DISTRIBUTION/AVAILABILITY OF REPORT <b>Approved for public release; distribution unlimited.</b>		
2b DECLASSIFICATION/DOWNGRADING SCHEDULE					
4 PERFORMING ORGANIZATION REPORT NUMBER(S) <b>NRL Memorandum Report 6499</b>			5 MONITORING ORGANIZATION REPORT NUMBER(S)		
6a NAME OF PERFORMING ORGANIZATION <b>Naval Research Laboratory</b>		6b OFFICE SYMBOL (If applicable) <b>Code 4430</b>	7a NAME OF MONITORING ORGANIZATION		
6c ADDRESS (City, State, and ZIP Code) <b>Washington, DC 20375-5000</b>			7b ADDRESS (City, State, and ZIP Code)		
8a NAME OF FUNDING/SPONSORING ORGANIZATION <b>Office of Naval Research</b>		8b OFFICE SYMBOL (If applicable)	9 PROCUREMENT INSTRUMENT IDENTIFICATION NUMBER		
8c ADDRESS (City, State, and ZIP Code) <b>Arlington, VA 22217</b>			10 SOURCE OF FUNDING NUMBERS		
	PROGRAM ELEMENT NO <b>61153N</b>	PROJECT NO	TASK NO <b>RR23-01-41</b>	WORK UNIT ACCESSION NO <b>DN158-015</b>	
11 TITLE (Include Security Classification) <b>Evaluation of the Near-Wall <math>k-\epsilon</math> Turbulence Model by Comparison with Direct Simulations of Turbulent Channel Flow</b>					
12 PERSONAL AUTHOR(S) <b>Miner, E.W., Swain, T.F. Jr., Handler, R.A. and Leighton, R.I.</b>					
13a TYPE OF REPORT <b>Interim</b>		13b TIME COVERED FROM <b>1/1</b> TO <b>present</b>		14 DATE OF REPORT (Year, Month, Day) <b>1989 September 7</b>	15 PAGE COUNT <b>37</b>
16 SUPPLEMENTARY NOTATION					
17 COSATI CODES			18 SUBJECT TERMS (Continue on reverse if necessary and identify by block number)		
FIELD	GROUP	SUB-GROUP	Turbulence modeling Two equation models		
			Low Reynolds number turbulence		
			Wall damping Direct simulation data		
19 ABSTRACT (Continue on reverse if necessary and identify by block number) <p>Handler, Hendricks and Leighton have recently reported results for the direct numerical simulation (DNS) of a turbulent channel flow at moderate Reynolds number. These data are used to evaluate the terms in the exact and modeled transport equations for the turbulence kinetic energy, <math>k</math>, and the isotropic dissipation function, <math>\epsilon</math>. Both transport equations show significant imbalances in the sums of the modeled terms in the high shear region near the channel walls. The model for the eddy viscosity is found to yield distributions for the modeled shear and production terms which do not agree well with the distributions calculated from the DNS data. The source of the imbalance is attributed to the wall damping function, <math>f_\mu</math>, which is required in eddy viscosity models for turbulent flows near walls. Several models for <math>f_\mu</math> are examined, and it is found</p> <p style="text-align: right;">(Continues)</p>					
20 DISTRIBUTION/AVAILABILITY OF ABSTRACT <input checked="" type="checkbox"/> UNCLASSIFIED/UNLIMITED <input type="checkbox"/> SAME AS RPT <input type="checkbox"/> DTIC USERS			21 ABSTRACT SECURITY CLASSIFICATION <b>UNCLASSIFIED</b>		
22a NAME OF RESPONSIBLE INDIVIDUAL <b>E. Wade Miner</b>			22b TELEPHONE (Include Area Code) <b>(202) 767-3389</b>	22c OFFICE SYMBOL <b>Code 4430</b>	

19. ABSTRACTS (Continued)

that the models do not vary across the channel as does  $f_\mu$  when evaluated from the DNS data. The Lam-Bremhorst model is found to give reasonable agreement with the DNS data. The standard van Driest model is found to give better agreement with the DNS data. Modification of the van Driest model to include an effective origin improves agreement and gives very good agreement between the modeled shear and the shear calculated from the DNS data.



# EVALUATION OF THE NEAR-WALL $k-\epsilon$ TURBULENCE MODEL BY COMPARISON WITH DIRECT SIMULATIONS OF TURBULENT CHANNEL FLOW

## I. INTRODUCTION

During the past three decades the fluid dynamics community has focused much of its attention on the development of techniques and capabilities for the calculation of turbulent flow fields. Increases in available computational capabilities have permitted researchers to develop and test increasingly sophisticated and complete models for the numerical simulation of turbulent flows. The state of the art has reached a point where direct numerical simulations of turbulent flows at low-to-moderate Reynolds numbers are feasible. Such work has been reported in several studies including those by Kim, Moin and Moser (1987) and Handler, Hendricks and Leighton (1989), hereinafter referred to as KMM and HHL, respectively. In these simulations, the unsteady Navier-Stokes equations are solved numerically. All essential scales of the turbulent flow are resolved and no subgrid modeling of the turbulence is employed. Such calculations, however, are feasible only for research purposes, and calculations of turbulent flows for engineering purposes utilize the time-averaged Navier-Stokes equations coupled with some level of turbulence modeling.

For many applications, the model of choice is the two equation  $k - \epsilon$  model. This model for turbulence transport came into use in the early 1970's based largely on the work of Hanjalić and Launder (1972) and Launder, Reece and Rodi (1975) and became a standard because of its relative simplicity and success in providing good predictions for a large range of turbulent flows. In spite of some significant shortcomings in the  $k - \epsilon$  model, it still retains a position as the standard for comparison.

In the development of the  $k - \epsilon$  model, attention was focused on high Reynolds number flows, such as thin shear layers, and the constants in the model were chosen to give agreement with experimental data. Consequently, the predictive capabilities of the model are best for strongly turbulent flows. For flows near fixed surfaces, adjustments to the model are needed. In Hanjalić and Launder (1972) and Launder, Reece and Rodi (1975), boundary layer flows were treated by matching the high Reynolds number flow with wall functions, e.g. "law-of-the-wall" profiles, at the first grid point away from the wall. In that way, the model did not have to be directly modified for the low Reynolds number flow adjacent to the wall. In work since then, Hanjalić and Launder (1976) and a number of researchers have proposed extensions to the basic high Reynolds number model that would enable the  $k - \epsilon$  model to be directly used all the way to the wall. Patel, Rodi and Scheuerer (1985) review a number of near-wall models and found that while the better ones did quite well, there were still areas where improvement was needed. One of the limitations in the development of near-wall models has been the difficulty in making accurate and reliable measurements of the flow quantities near the wall and the fact that some of the correlations that are needed in improving the  $k - \epsilon$  model cannot be obtained experimentally.

Data from direct numerical simulations of turbulent flows can be used in place of experimental data in evaluating and improving the near-wall turbulence models. Mansour, Kim and Moin (1988) have used the data of Kim, Moin and Moser (1987) to analyze some of the terms in the modeled transport equations for the Reynolds stresses. In this study, we use the direct simulation data of Handler, Hendricks and Leighton (1989) to examine the terms in the  $k - \epsilon$  model with emphasis on the behavior of the terms near the wall.

## II. DIRECT NUMERICAL SIMULATION

Numerical methods are being developed at the U. S. Naval Research Laboratory (NRL) for the direct numerical simulation (DNS) of turbulent flows. Much of the background for this effort is provided in the study by HHL. In their report, HHL review the numerical methods which are currently in vogue and present the results of applying these methods to the computation of turbulent channel flows. Several calculations parameterized by the extent of the physical domain, grid resolution, and Reynolds number are described. In this study, we use the Chan1.1 data of HHL. This is one of their lower resolution (spatial) data sets; however, it is one for which complete velocity and pressure are available at widely spaced time intervals, thus insuring that the separate realizations are statistically independent.

In units of channel half-width,  $h$ , the channel dimensions are  $2 \times 5 \times 5$  in the vertical ( $x_2$ ), the streamwise ( $x_1$ ) and lateral ( $x_3$ ) directions respectively. The flow is computed with  $16 \times 64$  evenly spaced grid points in the horizontal ( $x_1 - x_3$ ) plane and 33 points with Chebyshev scaling are used in the  $x_2$  direction. The Reynolds number,  $Re$ , is 2215 based on  $h$  and  $U_0$ , the initial laminar centerline velocity. The governing equations are nondimensionalized by the wall shear velocity, a viscous length unit and a viscous time unit. The wall shear velocity,  $u_\tau$ , is given by

$$u_\tau = \left[ \nu \frac{\partial \bar{U}_1}{\partial x_2} \Big|_w \right]^{\frac{1}{2}}.$$

The viscous length unit (or wall unit) is  $l_v = \nu/u_\tau$  and the viscous time unit is  $t_v = \nu/u_\tau^2$ . In the nondimensionalized units, the Reynolds number based on the wall shear velocity is 125. This is lower than the wall Reynolds number of 180 for the KMM data and the grid resolution of the Chan 1.1 data is lower. HHL conclude, however, that the mean statistics of their data set compare well with experiment and with the more highly resolved data of KMM insofar as one-point statistics are concerned.

The equations are solved using a pseudospectral method in which Chebyshev expansion is used in the wall normal ( $x_2$ ) direction and Fourier series are used in the streamwise ( $x_1$ ) and spanwise ( $x_3$ ) directions. The domain size in wall units is 640, 250 and 640 in the  $x_1$ ,  $x_2$  and  $x_3$  directions, respectively. In the  $x_2$  direction, the use of Chebyshev polynomials gives a variable step size, with  $\Delta x_2 \approx 0.6$  at the wall and  $\Delta x_2 \approx 12$  at the channel center. In the  $x_1$  and  $x_3$  directions the step size is uniform and is  $\Delta x_1 \approx 40$  and  $\Delta x_3 \approx 10$ . In the direct numerical simulation used in the present work, there are 33 distinct realizations of the velocity and pressure fields which are separated by 50 viscous time units. This separation in time is sufficient to insure that each realization of the fields is statistically independent.

We denote the instantaneous values of variables by uppercase symbols, the time averaged values with an overbar, and the fluctuations from the time averages by lowercase symbols so that, for example,

$$U_i(t) = \bar{U}_i + u_i(t) \quad \text{and} \quad P(t) = \bar{P} + p(t).$$

Also, we denote the turbulence intensities as  $u'_i = \sqrt{u_i'^2}$ . The velocity field in the channel is periodic in the  $x_1$  and  $x_3$  directions so that averaging over the  $x_1 - x_3$  plane at each value of  $x_2$  gives dependent variable profiles which are functions of the wall normal coordinate ( $x_2$ ). Averages are obtained by summing the individual profiles over 33 separate realizations. Correlations of the fluctuating variables such as  $\overline{u_1 u_2}$  are computed by forming the product at each grid point in the domain, averaging over the  $x_1 - x_3$  plane, and then averaging over the 33 realizations.

The primary averaged data from the direct numerical simulation of channel flow by HHL are shown in Figs. 1 and 2. Figure 1 shows the mean streamwise velocity  $\overline{U_1}$  and the root mean square of the pressure fluctuations  $p'$ . The velocity profile shows a fully developed turbulent flow profile with channel center value of 17. The rms of the pressure fluctuations show peaks of 1.9 at  $y/h = \pm 100$ . At the channel center,  $p'$  has a minimum value less than 1.0. The values at the walls are between 1.2 and 1.3. The wall values are lower than those reported by KMM (1.5), and the difference is attributable to the lower Reynolds number of the HHL simulation. Figure 2 shows the turbulence intensities,  $u'_1$ ,  $u'_2$  and  $u'_3$ , and the Reynolds shear stress,  $\overline{u_1 u_2}$ . It is noted by HHL that the location of the peak values of  $u'_i$  are in excellent agreement with the data of KMM and experimental data, although the peak values are slightly lower. The overall agreement between the HHL data and KMM data is good. The Reynolds shear stress,  $\overline{u_1 u_2}$ , shows peak values of  $\pm 0.65$  at  $y/h = \pm 95$  and linear variation over the interval  $-85 < y/h < 85$ . The averaged data in Figs. 1 and 2 exhibit good overall symmetry between the channel walls.

### III. THE $k - \epsilon$ TRANSPORT EQUATIONS

#### Exact Transport Equations

The two equation  $k - \epsilon$  model for turbulent flow requires transport equations for the turbulence kinetic energy,  $k$ , and for  $\epsilon$ , the rate of dissipation of turbulence energy. The exact equation for the transport of turbulence kinetic energy is obtained from the sum of the transport equations for the three normal Reynolds stresses. With a slight rearrangement, the  $k$  transport equation in indicial notation as given by Hinze (1975) is,

$$\begin{aligned}
\frac{Dk}{Dt} = & \text{(1)} \quad -\overline{u_i u_j} \frac{\partial \overline{U}_j}{\partial x_i} \quad \text{(2)} \quad - \frac{\partial}{\partial x_i} \left( \overline{u_i k'} \right) \quad \text{(3)} \quad - \frac{\partial}{\partial x_i} \left( \overline{u_i \frac{p}{\rho}} \right) \\
& + \nu \frac{\partial}{\partial x_i} \overline{u_j \left( \frac{\partial u_i}{\partial x_j} + \frac{\partial u_j}{\partial x_i} \right)} \quad \text{(4)} \quad - \nu \overline{\left( \frac{\partial u_i}{\partial x_j} + \frac{\partial u_j}{\partial x_i} \right) \frac{\partial u_j}{\partial x_i}} \quad \text{(5)}
\end{aligned} \tag{1}$$

where  $k'$  is half the sum of the normal stresses and  $k$  is its averaged value. It should be noted here that for the channel flow simulations the mean flow is homogeneous in the horizontal coordinate directions so that  $\overline{U}_1 = f(x_2)$  and  $\overline{U}_2 = \overline{U}_3 = 0$ . Because of symmetry with respect to planes normal to the spanwise direction, all correlations involving  $u_3$  and uneven derivatives with respect to  $x_3$  are zero.

The terms on the right hand side correspond to (1) production of turbulence kinetic energy, (2) transport of turbulence energy (3) transport of the pressure fluctuations, (4) viscous diffusion and (5) viscous dissipation. For an incompressible fluid, terms (4) and (5) can be written in the alternate form,

$$\frac{Dk}{Dt} = (1) + (2) + (3) + \nu \frac{\partial^2}{\partial x_i \partial x_i} k \quad \text{(4)} \quad - \nu \frac{\partial u_j}{\partial x_i} \frac{\partial u_j}{\partial x_i} \quad \text{(5)} \tag{2}$$

While the sum of terms (4) and (5) is the same in Eqs. 1 and 2, the individual terms are not equivalent. Term (5) in Eq. 1 is the full dissipation term and term (5) in Eq. 2 is the dissipation only in homogeneous turbulence. It is the latter term which is modeled in the  $k - \epsilon$  transport equations.

The exact transport equation for the dissipation rate term is derived from the unsteady Navier-Stokes equations. We use the form given by Hanjalić and Launder (1976),

$$\begin{aligned}
\frac{D\epsilon}{Dt} = & \text{(1)} \quad -2\nu \frac{\partial u_i}{\partial x_k} \frac{\partial u_i}{\partial x_l} \frac{\partial u_k}{\partial x_l} \quad \text{(2)} \quad -2 \overline{\left( \nu \frac{\partial^2 u_i}{\partial x_k \partial x_l} \right)^2} \quad \text{(3)} \quad - \frac{\partial}{\partial x_k} \left\{ \overline{u_k \epsilon'} + \frac{2\nu}{\rho} \frac{\partial u_k}{\partial x_l} \frac{\partial p}{\partial x_l} - \nu \frac{\partial \epsilon}{\partial x_k} \right\} \\
& - 2\nu \left\{ \frac{\partial u_i}{\partial x_l} \frac{\partial u_k}{\partial x_l} + \frac{\partial u_l}{\partial x_i} \frac{\partial u_l}{\partial x_k} \right\} \frac{\partial \overline{U}_i}{\partial x_k} \quad \text{(6)} \quad \text{(7)} \quad - 2\nu \overline{u_k \frac{\partial u_i}{\partial x_l} \frac{\partial^2 \overline{U}_i}{\partial x_k \partial x_l}} \quad \text{(8)}
\end{aligned} \tag{3}$$

where

$$\epsilon = \overline{\frac{\partial u_i}{\partial x_j} \frac{\partial u_i}{\partial x_j}} \quad \text{and} \quad \epsilon' = \frac{\partial u_i}{\partial x_j} \frac{\partial u_i}{\partial x_j}.$$

The first term on the right hand side of Eq. 3 represents turbulent production of  $\epsilon$ . Term (2) represents dissipation of  $\epsilon$ . The terms in the first pair of braces, terms (3), (4) and (5), represent turbulent transport, pressure transport and viscous diffusion. The last three terms, terms (6), (7) and (8), are production terms.

The individual terms in Eqs. 1-3 have been calculated from the DNS data of HHL. Products such as  $u_i u_j$  are formed at each grid point in the domain, the correlation is then averaged over the  $x_1 - x_3$  plane giving a profile in  $x_2$ . The  $x_2$  profiles are then averaged over the 33 realizations in the saved data sets. In forming the averages of the terms, we make use of the symmetry (in the mean) of the channel flow about the center line. In the following figures, we use the wall normal distance  $y^+$  with origin at the wall whereas in the preceding figures we used  $y/h$  with origin at the channel center.

Figure 3 shows the sums of terms (4) and (5) in Eqs. 1 and 2. The agreement between the sums of these terms is nearly exact, an indication of the fidelity of the simulation in maintaining a divergence free flow. Comparison of terms (5) in the two equations shows only slightly greater differences than is seen in the sums of the terms. The individual terms in Eq. 2 are shown in Fig. 4. These data agree very well with the data presented by Mansour, Kim and Moin (1988), hereinafter referred to as MKM, with the differences (small) being attributable primarily to the differences in resolution of the two calculations and to a lesser extent to the differences in Reynolds numbers. Both HHL and KMM make extensive comparisons with experimental data and find very good agreement, and such comparisons are not included herein. The interested reader may refer to those sources.

As seen from Fig. 5, across most of the channel, the principal contribution to the transport of  $\epsilon$  comes from terms (1) and (2). Near the wall (for  $y^+ < 25$ ) terms (6) and (7) become significant contributors and very near the wall (for  $y^+ < 3$ ), term (5) becomes a major contributor. At the wall, it is term (5) which balances term (2). The other three terms ((3), (4) and (8)) contribute very little to the transport of  $\epsilon$  in the channel and are not shown in this figure. Except for the small differences due to resolution and Reynolds number differences, these data agree nearly exactly with the corresponding data of MKM.

For engineering calculations of turbulent flows, the  $k - \epsilon$  model is adequate for many applications, but the terms involving the fluctuating velocity and pressure components must be modeled. The models which are in use have been developed based on

order of magnitude analysis of the transport equations and contain empirical constants which have been determined from experimental data. The experimental data base is incomplete because of difficulties of measuring some of the terms in the exact equations. The data from the direct simulations permit a precise examination of the terms in the transport equations and a new evaluation of the empirical constants in the turbulence models.

### Modeled Transport Equations

In modeling the terms of the  $k$  transport equations, terms (2) and (3) are taken together as the diffusional flux of  $k$  and assumed proportional to the gradient of  $k$ . Rodi (1980) gives

$$\overline{u_i \left( k + \frac{p}{\rho} \right)} = \frac{\nu_t}{\sigma_k} \frac{\partial k}{\partial x_i} \quad (4)$$

with  $\sigma_k$  an empirical diffusion constant. Term (4) of Eq. 2 is easily combined with Eq. 4, and term (5) is simply  $\epsilon$ . The Reynolds stresses  $\overline{u_i u_j}$  are modeled using the Boussinesq eddy viscosity relation

$$-\overline{u_i u_j} = \nu_t \left( \frac{\partial \overline{U}_i}{\partial x_j} + \frac{\partial \overline{U}_j}{\partial x_i} \right) - \frac{2}{3} k \delta_{ij} \quad (5)$$

with  $\delta_{ij}$  the Kronecker delta. The eddy viscosity, turbulence kinetic energy and the rate of dissipation of turbulence kinetic energy are related by

$$\nu_t = C_\mu \frac{k^2}{\epsilon} \quad (6)$$

where  $C_\mu$  is a constant. This expression for  $\nu_t$  yields good agreement for flows such as thin shear layers, but for turbulent flow next to a wall,  $C_\mu$  is not constant or a wall damping function needs to be included. Patel, Rodi and Scheuerer (1985) use the model

$$\nu_t = C_\mu f_\mu \frac{k^2}{\epsilon} \quad (7)$$

with the functional form of  $f_\mu$  to be determined by comparison with experimental data. The modeled form of the  $k$  transport equation then becomes

$$\frac{Dk}{Dt} = \frac{\partial}{\partial x_i} \left[ \left( \nu + \frac{\nu_t}{\sigma_k} \right) \frac{\partial k}{\partial x_i} \right] + \mathcal{P} - \epsilon \quad (8)$$

with

$$\mathcal{P} = \nu_t \left( \frac{\partial \bar{U}_i}{\partial x_j} + \frac{\partial \bar{U}_j}{\partial x_i} \right) \frac{\partial \bar{U}_i}{\partial x_j}. \quad (9)$$

The steps in developing the model for the  $\epsilon$  transport equations are quite complex and are not detailed here. Hanjalić and Launder (1976) give the following form which retains a direct Reynolds stress expression

$$\frac{D\epsilon}{Dt} = C_{\epsilon 1} \frac{\epsilon}{k} \mathcal{P} - C_{\epsilon 2} \frac{\epsilon^2}{k} - C_{\epsilon} \frac{\partial}{\partial x_k} \left\{ \frac{k}{\epsilon} \overline{u_k u_l} \frac{\partial \epsilon}{\partial x_l} \right\}. \quad (10)$$

They note that at a wall, the  $\epsilon^2/k$  term is unbounded, since  $\epsilon$  has a finite value at the wall and  $k \rightarrow 0$ . They eliminate this difficulty by replacing  $\epsilon^2$  by  $\epsilon \tilde{\epsilon}$  where  $\tilde{\epsilon}$  is defined by

$$\tilde{\epsilon} = \epsilon - 2\nu \left( \frac{\partial k^{1/2}}{\partial x_l} \right)^2 \quad (11)$$

and show that  $\tilde{\epsilon}/k$  approaches a finite value at the wall which ensures that  $\epsilon \tilde{\epsilon}/k$  is bounded as  $y^+ \rightarrow 0$ .

For the  $k - \epsilon$  model equations, the last term in Eq. 10 is written as a diffusion term with  $\overline{u_i u_j} k / \epsilon$  replaced by  $-\nu_t / \sigma_\epsilon$ , where  $\sigma_\epsilon$  is an empirical dissipation constant. This term is then combined with term (5) of Eq. 3. The modeled transport equation for  $\epsilon$  takes the form

$$\frac{D\epsilon}{Dt} = \frac{\partial}{\partial x_i} \left[ \left( \nu + \frac{\nu_t}{\sigma_\epsilon} \right) \frac{\partial \epsilon}{\partial x_i} \right] + C_{\epsilon 1} \frac{\epsilon}{k} \mathcal{P} - C_{\epsilon 2} \frac{\epsilon \tilde{\epsilon}}{k}, \quad (12)$$

with  $\nu_t$  and  $\mathcal{P}$  as given above. Commonly accepted values of the constants  $\sigma_k$ ,  $\sigma_\epsilon$ ,  $C_{\epsilon 1}$  and  $C_{\epsilon 2}$  are 1.0, 1.3, 1.44 and 1.92, respectively.

For the channel,  $\bar{U}_2$  and  $\bar{U}_3$  are zero as are the derivatives of the averaged turbulence variables in the  $x_1$  and  $x_3$  directions. The modeled transport equations thus reduce to the following form

$$\frac{Dk}{Dt} = \frac{\partial}{\partial x_2} \left[ \left( \nu + \frac{\nu_t}{\sigma_k} \right) \frac{\partial k}{\partial x_2} \right] + \mathcal{P} - \epsilon \quad (13)$$

and

$$\frac{D\epsilon}{Dt} = \frac{\partial}{\partial x_2} \left[ \left( \nu + \frac{\nu_t}{\sigma_\epsilon} \right) \frac{\partial \epsilon}{\partial x_2} \right] + C_{\epsilon 1} \frac{\epsilon}{k} \mathcal{P} - C_{\epsilon 2} \frac{\epsilon \bar{\epsilon}}{k} \quad (14)$$

with

$$\mathcal{P} = \nu_t \frac{\partial \bar{U}_1}{\partial x_2} \frac{\partial \bar{U}_1}{\partial x_2} \quad (15)$$

and

$$-\overline{u_1 u_2} = \nu_t \frac{\partial \bar{U}_1}{\partial x_2}. \quad (16)$$

The eddy viscosity is given by Eq. 7. For thin shear flows  $C_\mu$  is a constant and a value of 0.09 is typical. Likewise, for thin shear flows,  $f_\mu = 1.0$ . For wall bounded flows,  $f_\mu$  is the wall damping function and is usually chosen to approach 1.0 when the flow is not influenced by the wall.

#### IV. EVALUATION OF THE $k - \epsilon$ MODEL

One of the significant differences between the  $k - \epsilon$  turbulence model and models which require additional transport equations is in the treatment on the Reynolds stress terms,  $\overline{u_i u_j}$ . In the models using separate equations for the transport of the Reynolds stresses, the  $\overline{u_i u_j}$  terms are solved as unknown variables. In the  $k - \epsilon$  model, the Reynolds stress terms are modeled using the eddy viscosity as given in Eqs. 7 and 16. The accuracy of this model is then central in considering the accuracy of the  $k - \epsilon$  model

If  $f_\mu$  is taken to be 1.0, the  $k - \epsilon$  model corresponds to a high Reynolds number model. Using the HHL data, we calculate the terms in each side of Eq. 16 with  $\nu_t$  given by Eq. 7,  $C_\mu = 0.09$  and  $f_\mu = 1.0$ . Figure 6 displays the two sides of Eq. 16 and we see that the equation applies very well in the center of the channel but that in the near-wall region the modeled term is much larger than the Reynolds stress computed from the DNS data. These data show that a damping term is required to bring the modeled Reynolds stress into better agreement with that calculated from the simulation data.

A number of wall damping models have been proposed. One of the simplest (and oldest) is that proposed by van Driest (1954) in which the damping depends only on the law-of-the-wall coordinate,  $y^+$ , and a constant of the turbulence,  $A^+$ . In that model, the appropriate damping function for the eddy viscosity is determined to be

$$f_\mu = \left[ 1 - \exp(-y^+/A^+) \right]^2. \quad (17)$$

This model has given excellent results for simple flows like flat plates, but has been judged inadequate for more complex flows, such as those with recirculation and those with pressure gradients. Many of the proposed alternatives to Eq. 17 depend upon a Reynolds number of turbulence, either  $R_y = \sqrt{k}y^+$ , or  $R_T = k^2/\epsilon$ , and do not depend solely upon  $y^+$ .

In the review of Patel, Rodi and Scheuerer (1985), eight different models for calculation of near-wall turbulent flows are discussed. They found that the model of Lam and Bremhorst (1981) provided the most reasonable wall damping for the experimental data they considered. In that model, the damping function is given by,

$$f_\mu = \left[ 1 - \exp(-0.0165R_y) \right]^2 \left( 1 + \frac{20.5}{R_T} \right). \quad (18)$$

Patel and his colleagues have since used the Lam-Bremhorst model for a number of turbulent flow calculations with good results (e.g. Chen and Patel, 1987).

In the review of Patel, et al.,  $C_\mu = 0.09$  was used for most of the models, including the Lam-Bremhorst model. Since 0.09 is a commonly accepted value for  $C_\mu$ , we use that value as the basis for comparison. Figure 7 shows the Reynolds shear stress as calculated from the DNS data and as modeled by Eqs. 16 and 7 using  $C_\mu = 0.09$  and  $f_\mu$  from Eq. 18. With this wall damping the modeled and exact shears have about the same peak value, but at different distances from the wall. However, the model gives too low a value for  $y^+ > 25$ .

Figures 8 and 9 show respectively the budgets for the terms in the modeled  $k$  and  $\epsilon$  transport equations using the wall damping function in Eq. 18. For the  $k$  transport equation, the diffusion term is very small in the center of the channel, then becomes more significant for  $y^+ < 30$ , peaks at  $y^+ = 15$ , changes sign and is large at the wall (due to the molecular viscosity). The production term is small in the center of the channel, starts to increase for  $y^+ < 50$ , peaks at a large value at  $y^+ = 15$  and goes to zero at the wall. The dissipation term is larger (with opposite sign) than the production term for  $50 < y^+ < 125$ , increases in magnitude as the wall is approached, and reaches its minimum at the wall, where it is balanced by the diffusion term. Also shown is the sum of the three modeled terms, and it is seen that there is significant imbalance. The source of imbalance is the contribution of the production term. For  $y^+ < 25$ , the production term contributes too much, and, for  $y^+ > 25$ , the production

term contributes too little. For the  $\epsilon$  transport equation, the character of the terms is like that of the terms of the  $k$  transport equation.

While good results have been obtained with the Lam-Bremhorst wall damping model (Chen and Patel, 1987), the amount of imbalance in the modeled forms of the transport equations suggests that the production term can be better modeled. We use the HHL data to determine the form that  $f_\mu$  should take and compare that with the form given by the Lam-Bremhorst model and other models. Equations 7 and 16 are combined to give

$$f_\mu = -\overline{u_1 u_2} \frac{\epsilon}{C_\mu k^2} \left[ \frac{\partial \overline{U}_1}{\partial x_2} \right]^{-1}, \quad (19)$$

with  $C_\mu$  to be chosen so that  $f_\mu$  goes to 1.0 at the channel center. We note that at the wall  $k = 0$  and at the channel center  $\partial \overline{U}_1 / \partial x_2 = 0$ . Therefore, we limit evaluation of Eq. 19 to the interval  $0 < y^+ < 125$ .

Figure 10 shows the distribution of  $f_\mu$ , across the half-channel, calculated from Eq. 19 and with  $C_\mu = 0.115$ , a value that allows  $f_\mu$  to approach 1.0 at the channel center. Also shown is  $f_\mu$  from Eq. 18. For  $10 < y^+ < 30$ , the model gives too large a value by up to about 70%. For  $y^+ > 30$ , the model gives as much as one fourth too low a value. We have examined how the values of the model change as the coefficients of  $R_T$  and  $R_y$  are changed. Since the second term of Eq. 18 is greater than one for all values of  $R_T$ , increases in the coefficient of  $R_y$  can give values of  $f_\mu$  greater than one at the channel center. We find that the coefficients given in Eq. 18 seem to give the best overall agreement between the model and  $f_\mu$  from the DNS data. What is needed for better agreement with the HHL data is a model which gives larger values of  $f_\mu$  for the middle portion of the channel and lower values near the wall. We have looked at a number of other wall damping models, including those considered by Patel, Rodi and Scheuerer (1985), that of Jones and Launder (1972) and that of Kim (1988). While we do not find good agreement between the models based on  $R_T$  and/or  $R_y$  and  $f_\mu$  calculated from the HHL data, the Lam-Bremhorst model does give better agreement with the HHL data than do the other models.

Figure 10 shows a characteristic of  $f_\mu$  which is seldom noted. As calculated from the DNS data using Eq. 19,  $f_\mu$  has a minimum value of 0.04 at  $y^+ = 6$  and  $f_\mu$  then increases toward the wall. Such a characteristic also appears in the  $f_\mu$  which Patel, et al. derived from experimental data and show in their Fig. 2. However, they do not comment on this characteristic. We have reproduced as the full rectangles in Fig. 10 some of the data from their Fig. 2. The experimental data for  $f_\mu$  are in good agreement

with the HHL data and show a non-zero minimum at about  $y^+ = 7$ . Expansion of the terms of Eq. 19 in Taylor series about  $y^+ = 0$  shows that for small  $y^+$ ,  $u_1 = ay^+ + \dots$ ,  $u_1 u_2 \rightarrow by^{+3} + \dots$ ,  $\epsilon' \rightarrow c + dy^+ + \dots$  and  $k' \rightarrow ey^{+2} + \dots$ . Since near the wall  $\partial \bar{U}_1 / \partial x_2$  is constant, the damping function in Eq. 19 must vary as  $g/y^+ + h + \dots$ . The result of this simple analysis is difficult to work with since it contains a singularity, but it does indicate that  $f_\mu$  should have a minimum located off the wall. None of the wall damping models vary as  $1/y^+$  for small  $y^+$  and most go to zero instead of to a non-zero minimum.

During the course of examining the wall damping models mentioned above, we also compared the model of van Driest (1954) given in Eq. 17 with the DNS data, and we find that the van Driest model agrees better with the HHL data than does the Lam-Bremhorst model. Figure 11 shows  $f_\mu$  from the HHL data and from Eq. 17 with  $A^+ = 26$  which is the commonly accepted value. We note that the model gives too large a value in the interval  $10 < y^+ < 50$  but that the shape of the distribution of  $f_\mu$  from the model and from the HHL data is similar. By introducing an effective origin for  $y^+$ , the modeled  $f_\mu$  and that from the HHL data can be brought into very close agreement. The use of an effective origin mimics the observed behavior that  $f_\mu$  possesses a minimum off the wall, however it does not produce a  $1/y^+$  variation. Figure 12 shows a comparison between  $f_\mu$  from the HHL data and from Eq. 17 with  $y^+$  replaced by  $y^+ - y_0^+$  and  $y_0^+ = 6$ . With this addition of an effective origin, the agreement between  $f_\mu$  from the data and from the van Driest model is good over all and is almost exact in the neighborhood of  $y^+ = 25$ . Near the wall, the model gives a value of zero at the effective origin, whereas the HHL data show a value of about 0.04. The model can be brought into closer agreement with the HHL data by introducing a minimum value,  $f_0$ . The modified damping function is then given by

$$f_\mu = f_0 + (1 - f_0) \left( 1 - \exp[-(y^+ - y_0^+)/A^+] \right)^2. \quad (20)$$

The introduction of  $f_0$  shifts the curve upwards and  $y_0^+$  needs to be correspondingly increased to maintain agreement with the direct simulation data. Figure 13 shows a comparison between  $f_\mu$  from the HHL data and from Eq. 20 with  $y_0^+ = 8$  and  $f_0 = 0.04$ . The agreement is seen to be very good. Also shown in this figure are the Patel, et al. data presented in Fig. 10. The modifications to the van Driest wall damping function are consistent with the experimental data and the direct simulation data.

With  $f_\mu$  as shown in Fig. 13, and with  $C_\mu = 0.115$ , the modeled shear agrees very well with the exact shear as is shown in Fig. 14. Also shown in Fig. 14 is the shear calculated with the unmodified van Driest damping function. With the unmodified

damping function,  $C_\mu$  is taken to be 0.09 for direct comparison with the modeled shear calculated with the Lam-Bremhorst model shown in Fig. 7. That comparison shows that the van Driest model gives a greater shear across all the channel. For  $y^+ < 25$ , the shear modeled with the Lam-Bremhorst damping function agrees better with the exact shear than does that with the Driest damping function. However, for  $y^+ > 25$ , the van Driest damping function yields the better agreement. Overall, the van Driest model gives better agreement with the exact shear from the HHL data than does the Lam-Bremhorst model.

Use of the modified van Driest model for  $f_\mu$  reduces the imbalance in the sum of the modeled terms in the  $k$  transport equation. Figure 15 shows the variation of the terms of the  $k$  transport equation modeled with the modified van Driest damping function. Comparison with Fig. 8 shows that the imbalance is reduced by more than a factor of two.

The DNS data also make it possible to evaluate the validity of one of the basic assumptions of developing the  $k - \epsilon$  model: that the production and dissipation of turbulence kinetic energy are in approximate balance. The production of turbulence kinetic energy is calculated from the DNS data using the equation

$$\mathcal{P} = -\overline{u_1 u_2} \frac{\partial \overline{U}_1}{\partial x_2}. \quad (21)$$

The variation across the channel of the ratio  $\mathcal{P}/\epsilon$  is shown in Fig. 16. Except for  $10 < y^+ < 35$ , the ratio is less than one and is zero at the wall and the channel center. At  $y^+ = 15$ ,  $\mathcal{P}/\epsilon$  has its peak value of approximately 1.9. Averaged across the channel,  $\mathcal{P}/\epsilon$  is less than one.

Rodi (1980) reports the results of considering a number of turbulent flows for which the ratio  $\mathcal{P}/\epsilon$  was not unity. In earlier work, he had found that the experimental data correlated with a function  $C_\mu = f(\mathcal{P}/\epsilon)$  whereby  $C_\mu$  varied inversely with  $\mathcal{P}/\epsilon$ . Denoting by  $C_\mu(y)$  the product of  $C_\mu$  and  $f_\mu$ , we show in Fig. 17 the values of  $C_\mu(y)$  plotted vs.  $\mathcal{P}/\epsilon$  with the omission of the 5 points nearest the wall. This shows a distribution of  $C_\mu(y)$  vs  $\mathcal{P}/\epsilon$  much like that given by Rodi except that  $C_\mu(y)$  is constant at about 0.11 for  $\mathcal{P}/\epsilon < 0.7$  instead of continuing to increase as  $\mathcal{P}/\epsilon \rightarrow 0$ .

## V. SUMMARY AND CONCLUSIONS

In this report, we have performed an evaluation of the  $k - \epsilon$  turbulence model using the direct numerical simulation data of Handler, Hendricks and Leighton for turbulent channel flow. With the DNS data, we have evaluated the terms of the exact  $k - \epsilon$

transport equations and have found nearly exact agreement with the budget data presented by Mansour, Kim and Moin. Evaluation of the terms of the modeled transport equations shows the necessity of using a wall damping function in the modeling of the eddy viscosity. From the HHL direct simulation data, we have determined the shape required for a damping function to obtain agreement between the modeled Reynolds shear stress and that calculated from the DNS data. We have shown that the well accepted Lam-Bremhorst wall damping model gives reasonable agreement with the DNS data.

We have also examined a number of other wall damping models. Those which are functions of the turbulence Reynolds numbers generally agree less well with the DNS function than does the Lam-Bremhorst model. We find that the standard van Driest wall damping model gives better agreement with the DNS data than the Lam-Bremhorst model. We further find that modifying the van Driest damping model to include an effective origin gives very good agreement between the modeled shear and the shear calculated from the HHL data.

## VI. ACKNOWLEDGEMENTS

This work was supported by the Fluid Dynamics 6.1 Task Area of the Naval Research Laboratory. The channel code used in the current work was originally developed by Professor John McLaughlin (Clarkson University) and was modified by Steven Lyons (University of Illinois). The code was also modified at the Naval Research Laboratory to run efficiently on a Cray XMP 24.

## VII. REFERENCES

- Chen, H. C. and Patel, V. C., 1987, "Practical Near-Wall Turbulence Models for Complex Flows Including Separation," AIAA-87-1300.
- Jones, W. P. and Launder, B. E., 1972, "The Prediction of Laminarization with a Two-Equation Model of Turbulence," *International Journal of Heat and Mass Transfer*, Vol. 15, pp. 301-314.
- Handler, R. A., Hendricks, E. W., and Leighton, R. I., 1989, "Low Reynolds Number Calculations of Turbulent Channel Flow: A General Discussion," NRL Memorandum Report 6410, Naval Research Laboratory, Washington, D. C.
- Hanjalić, K. and Launder, B. E., 1972, "A Reynolds stress model of turbulence and its application to thin shear flows," *Journal of Fluid Mechanics*, Vol. 52, part 4, pp. 609-638.

- Hanjalić, K. and Launder, B. E., 1976, "Contribution towards a Reynolds-stress closure for low-Reynolds-number turbulence." *Journal of Fluid Mechanics*, Vol. 74, part 4, pp. 593-610.
- Hinze, J. O., 1975, *Turbulence*, McGraw-Hill, New York.
- Kim, J., Moin, P., and Moser, R., 1987, "Turbulence statistics in fully developed channel flow at low Reynolds number," *Journal of Fluid Mechanics*, Vol. 177, pp. 133-166.
- Kim, S.-W., 1988, "A Near-Wall Turbulence Model and its Application to Fully Developed Turbulent Channel and Pipe Flows," NASA TM 101399 (ICOMP-88-20).
- Lam, C. K. G. and Bremhorst, K. A., 1981, "Modified Form of the  $k - \epsilon$ -Model for Predicting Wall Turbulence," *Journal of Fluids Engineering*, Vol. 103, pp. 456-460.
- Launder, B. E., Reece, G. J., and Rodi, W., 1975, "Progress in the development of a Reynolds-stress turbulence closure," *Journal of Fluid Mechanics*, Vol. 68, part 3, pp. 537-566.
- Mansour, N. N., Kim, J., and Moin, P., 1988, "Reynolds-stress and dissipation-rate budgets in a turbulent channel flow," *Journal of Fluid Mechanics*, Vol. 194, pp. 15-44.
- Patel, V. C., Rodi, W., and Scheuerer, G., 1985, "Turbulent Models for Near-Wall and Low Reynolds Number Flows: A Review," *AIAA Journal*, Vol. 23, No. 9, pp. 1308-1319.
- Rodi, W., 1980, *Turbulence Models and their Application in Hydraulics*, International Association for Hydraulic Research, Delft, Netherlands.
- van Driest, E. R., 1956, "On Turbulent Flow Near a Wall," *Journal of the Aeronautical Sciences*, Vol. 23, No. 11, pp. 1007-1011.

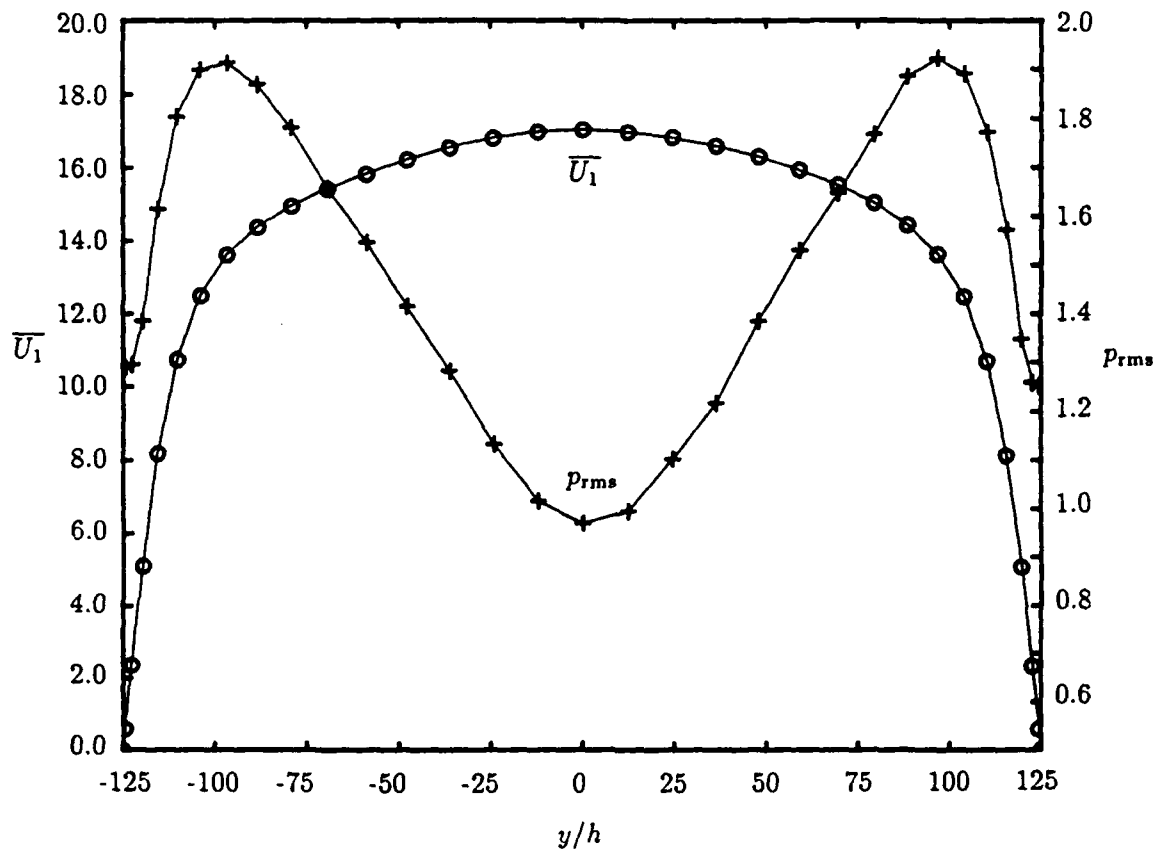


Fig. 1 — Profiles of mean streamwise velocity,  $\bar{U}_1$ , and root mean square of pressure fluctuations,  $p'$ , from the direct simulation data of Handler, Hendricks and Leighton (1989).

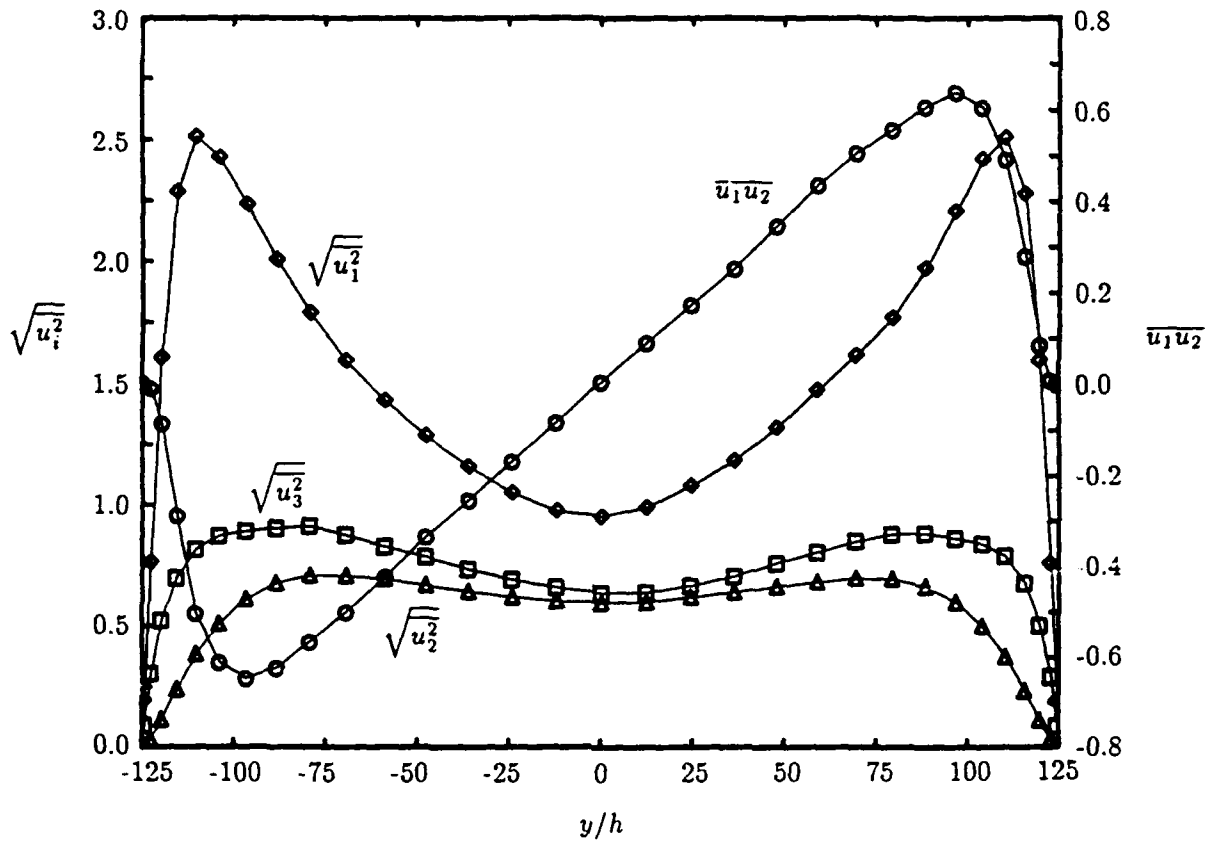


Fig. 2 — Profiles of turbulence intensities,  $\sqrt{u_i^2}$ , and Reynolds shear stress,  $\overline{u_1 u_2}$ , from the HHL data.

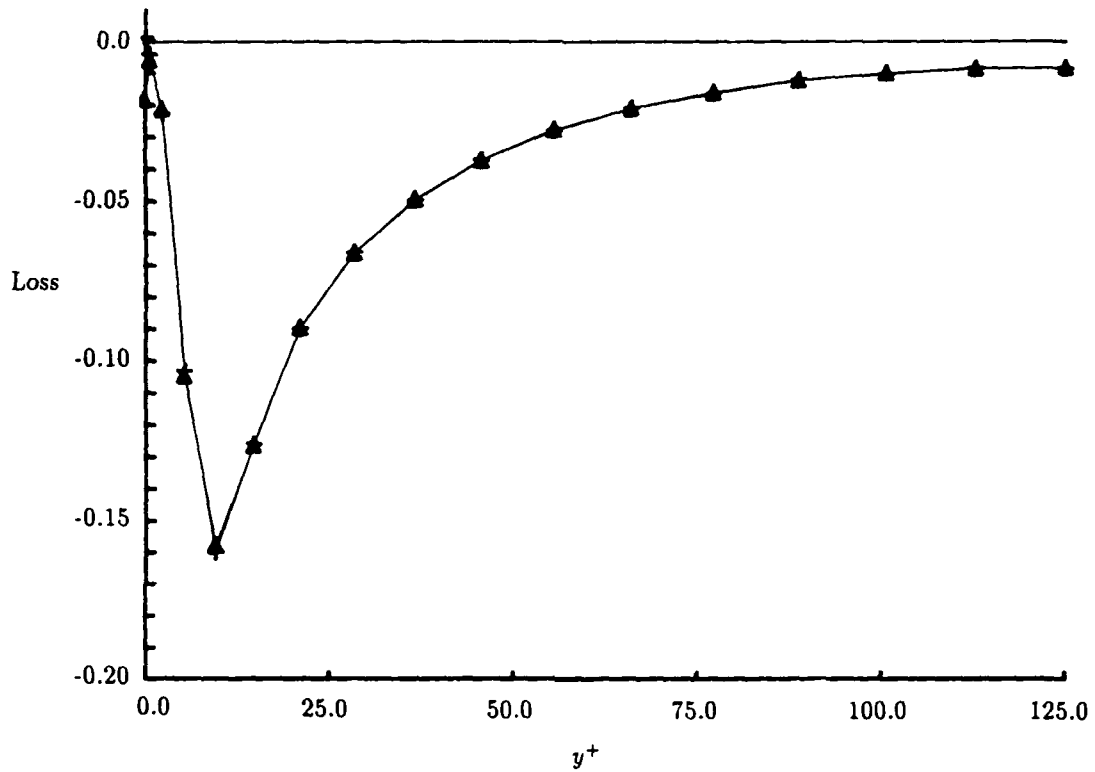


Fig. 3 — Comparison of the sum of the viscous terms in the two forms of the exact  $k$  transport equation. Terms (4) and (5) of Eq. 1 are shown as (+). Terms (4) and (5) of Eq. 2 are shown as ( $\Delta$ ).

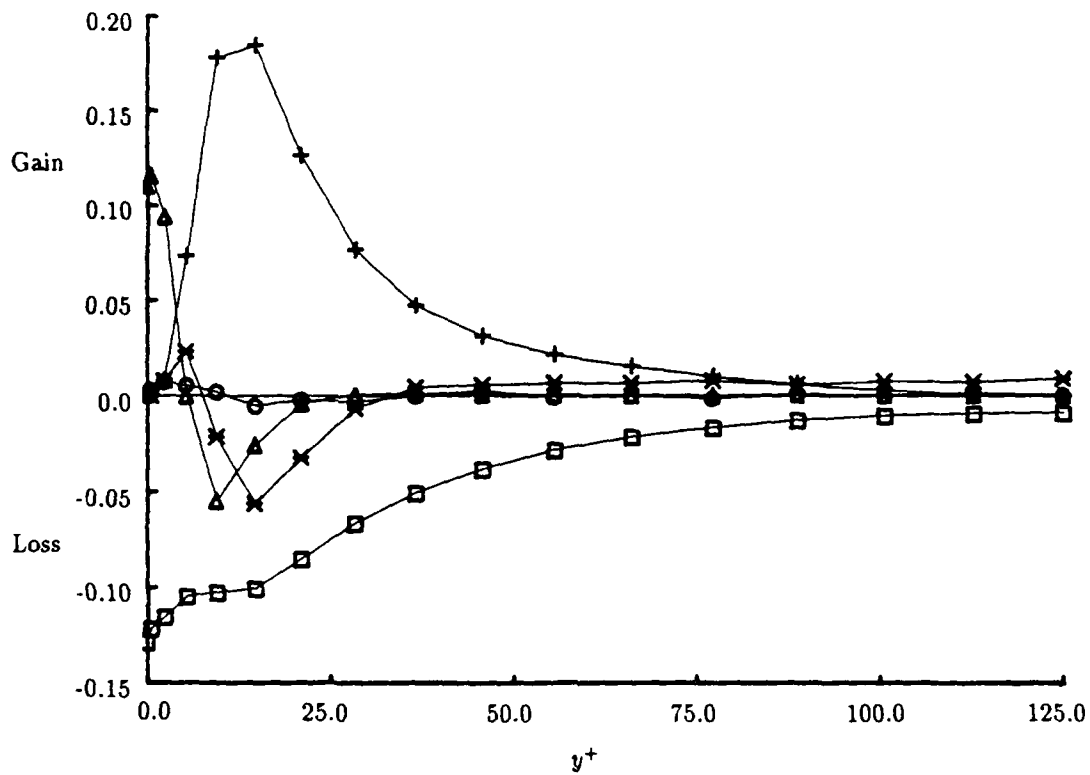


Fig. 4 — Budgets of the terms of the exact  $k$  transport equation for incompressible flow. Production term,  $P$ , (+); transport of turbulence energy (\*); transport of pressure fluctuations (O); viscous diffusion of  $k$  ( $\Delta$ ); and homogeneous viscous dissipation,  $\epsilon$ , ( $\square$ ).

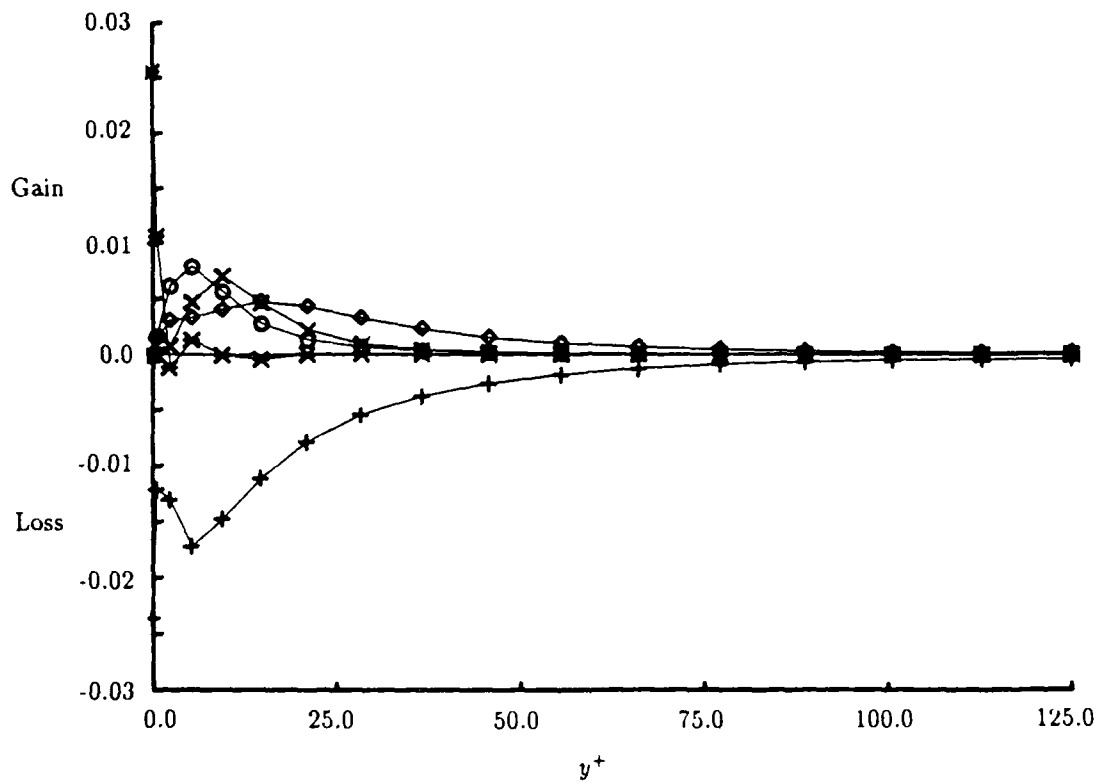


Fig. 5 — Budgets of the principal terms of the exact  $\epsilon$  transport equation. Turbulent production of  $\epsilon$  (◇); dissipation of  $\epsilon$  (+); viscous diffusion (\*); production terms: term (6), (○), and term (7), (×).

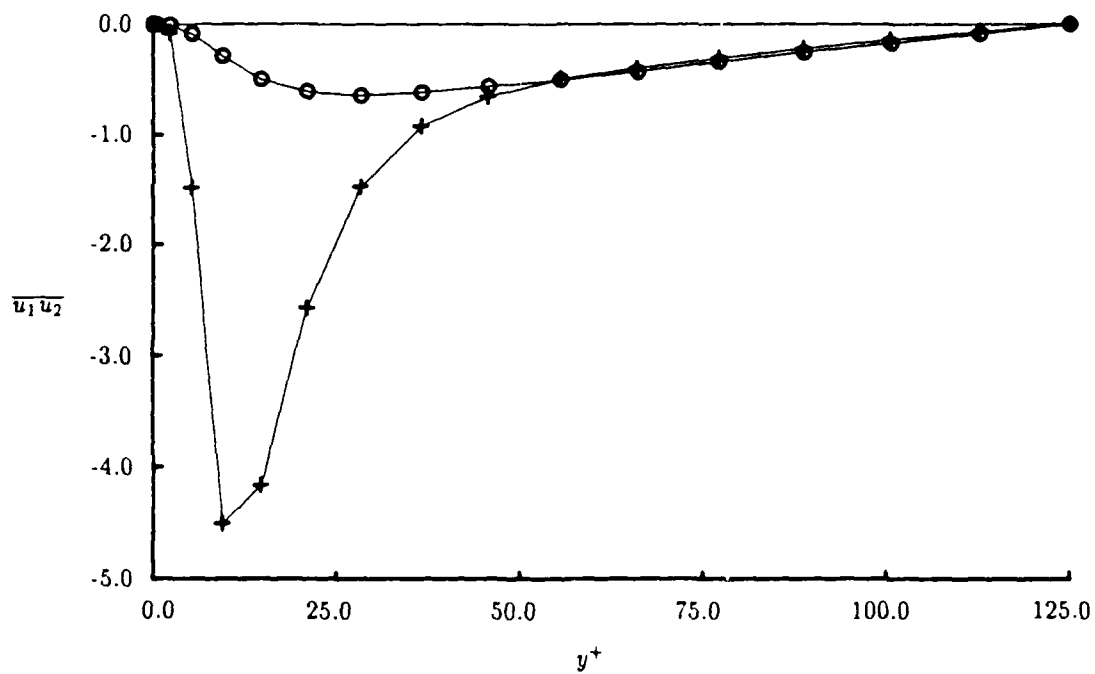


Fig. 6 — Comparison of the Reynolds shear stress,  $\overline{u_1 u_2}$ , calculated from the HHL data (○) and modeled by the eddy viscosity in Eq. 16 (+).

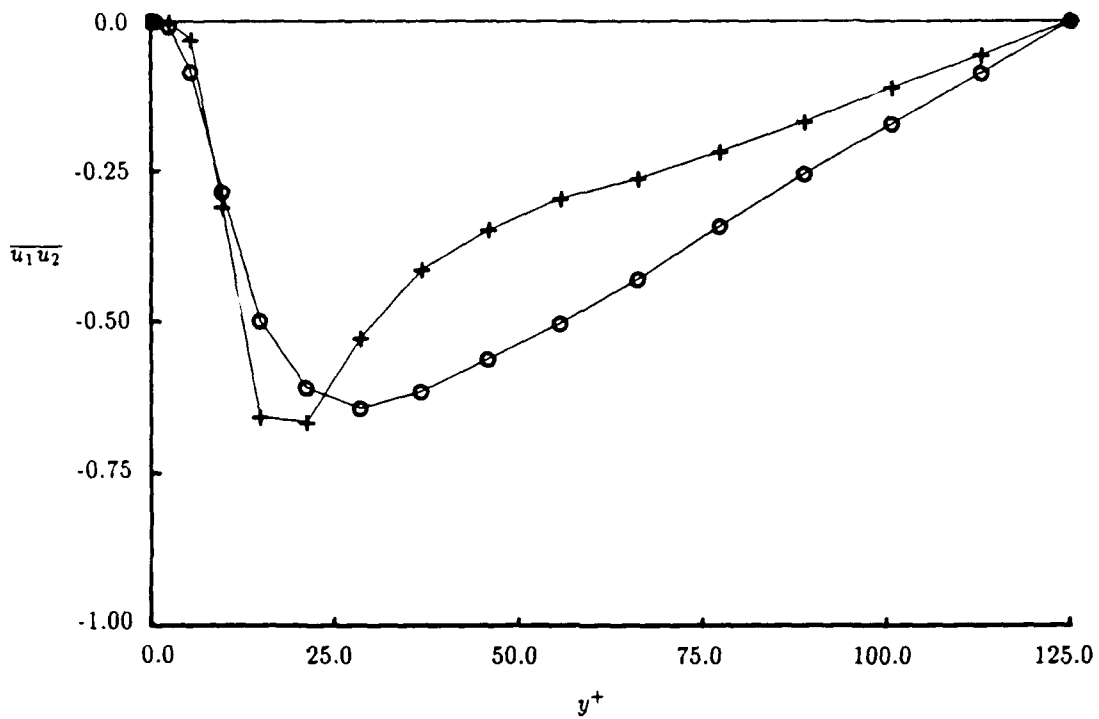


Fig. 7 — Comparison of the Reynolds shear stress,  $\overline{u_1 u_2}$ , calculated from the HHL data ( $\circ$ ) and modeled by the eddy viscosity with the Lam-Bremhorst wall damping function ( $+$ ).  $C_\mu = 0.09$ .

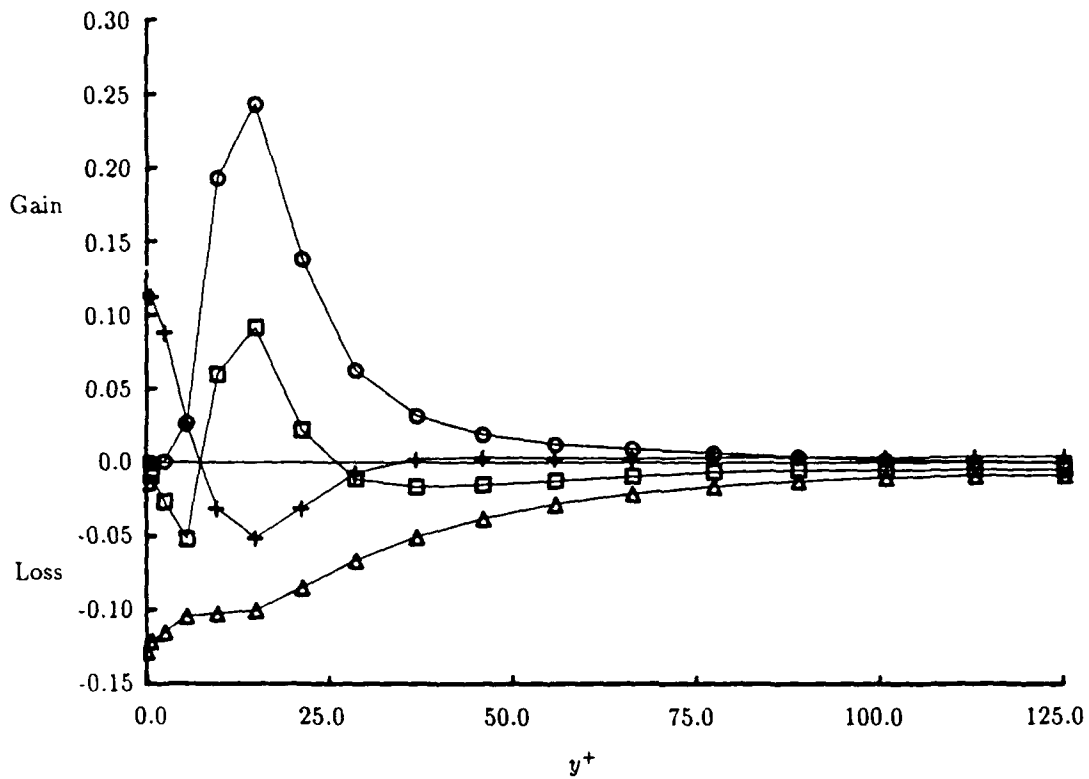


Fig. 8 — Budgets of the terms in the modeled transport equation for turbulence kinetic energy using the Lam-Bremhorst wall damping model. Dissipation term,  $\epsilon$ , ( $\Delta$ ); diffusion term (first term in Eq. 13) (+); production term,  $P$ , ( $\circ$ ); and sum of terms ( $\square$ ).  $C_x = 0.09$ .

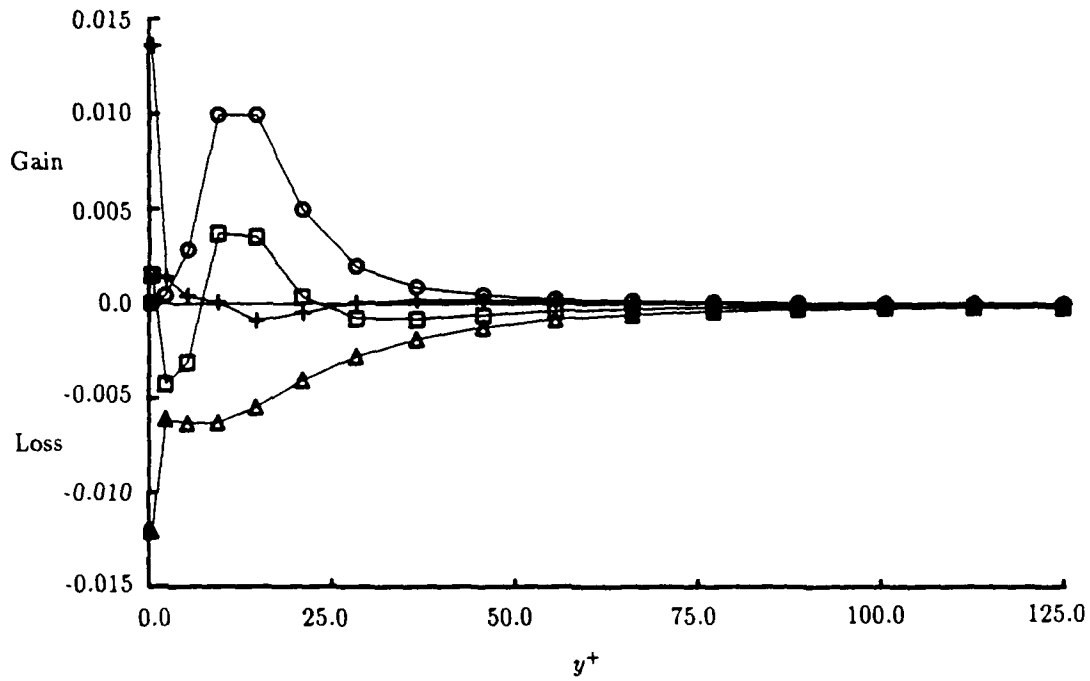


Fig. 9 — Budgets of the terms in the modeled transport equation for the homogeneous dissipation function using the Lam-Bremhorst wall damping model. Diffusion term (first term in Eq. 14) (+); production term,  $C_{e1}\epsilon P/k$ , (O); Dissipation term,  $C_{e2}\epsilon\tilde{\epsilon}/k$ , ( $\Delta$ ); and sum of terms ( $\square$ ).  $C_\mu = 0.09$ .

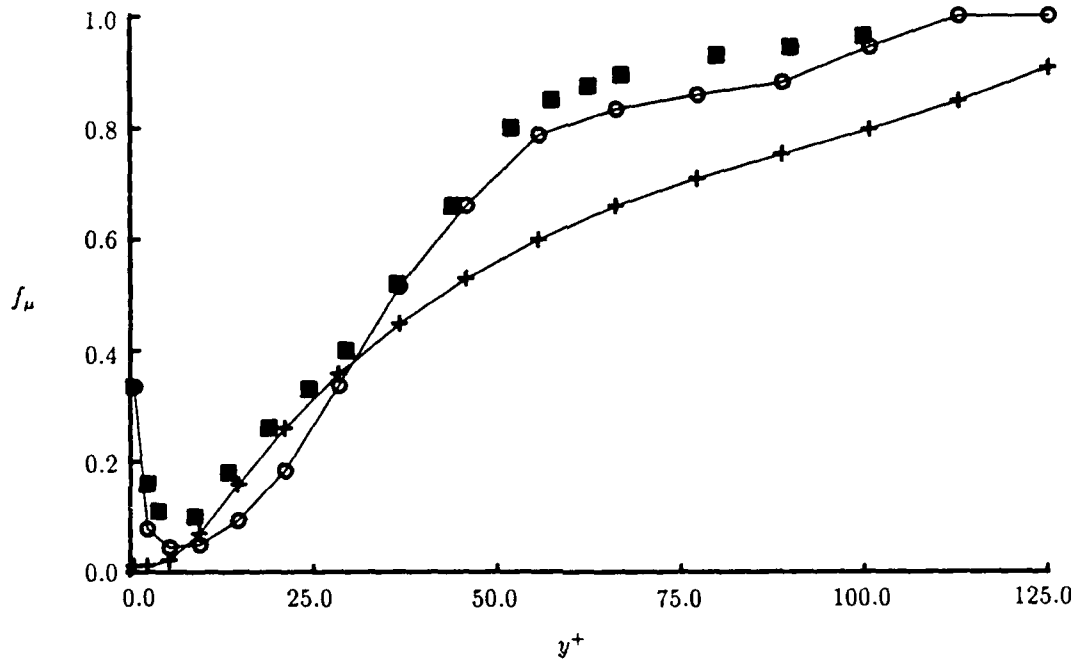


Fig. 10 — Comparison of the wall damping function,  $f_\mu$ , from the experimental data of Patel, et al. ( $\square$ ), calculated from the HHL data, Eq. 19, ( $\circ$ ), and from the Lam-Bremhorst model, Eq. 18, ( $+$ ). For HHL data,  $C_\mu = 0.115$  to give  $f_\mu = 1.0$  at channel center.

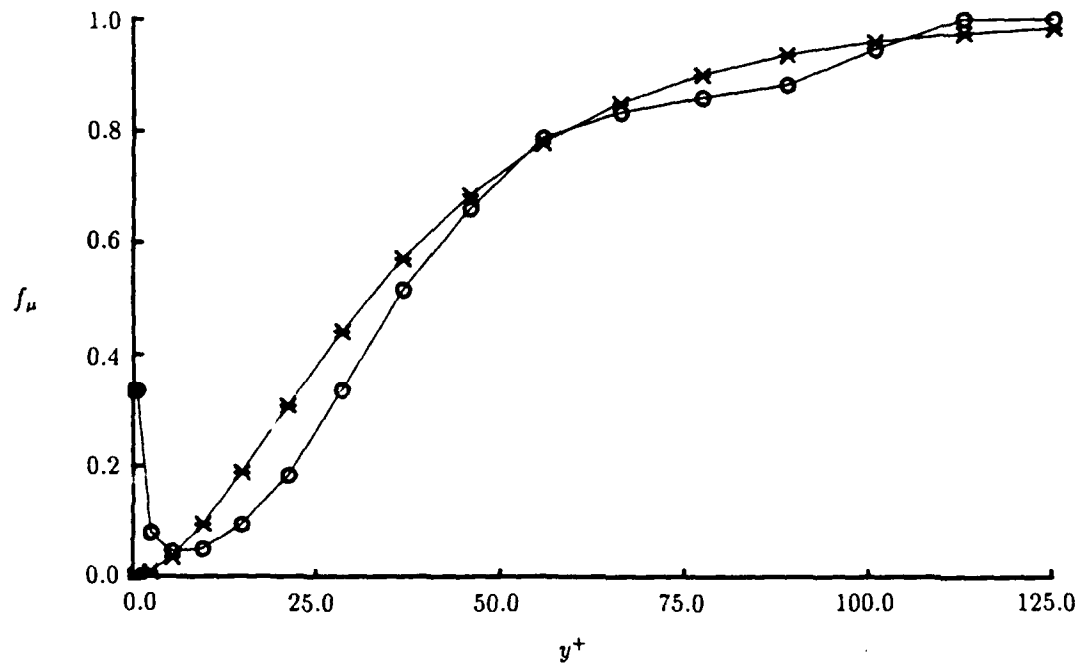


Fig. 11 — Comparison of the wall damping function,  $f_\mu$ , calculated from the HHL data, Eq. 19 with  $C_\mu = 0.115$ , ( $\circ$ ), and from the standard van Driest model, Eq. 17, ( $+$ ).

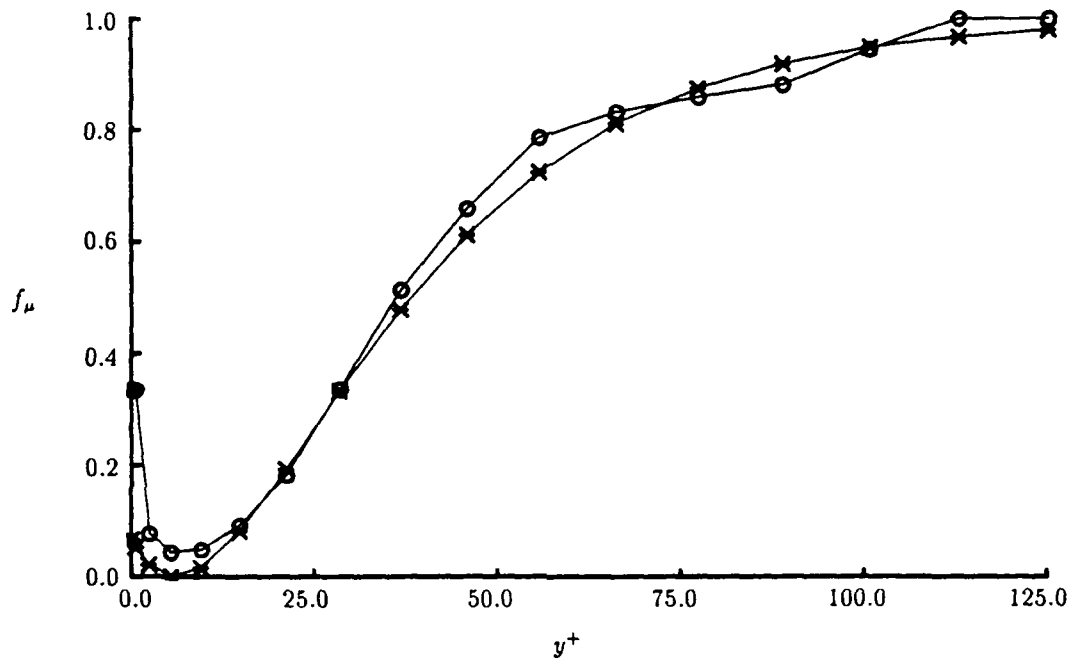


Fig. 12 — Comparison of the wall damping function,  $f_\mu$ , calculated from the HHL data, Eq. 19 with  $C_\mu = 0.115$ , (○), and from the modified van Driest model with  $y_0^+ = 6$ , (+).

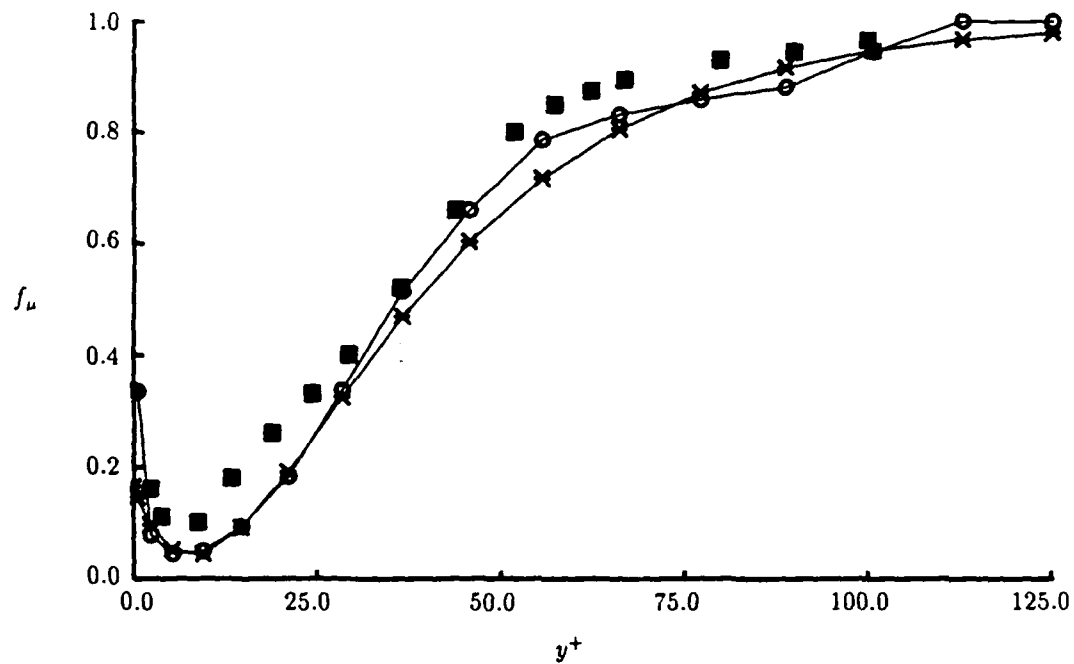


Fig. 13 — Comparison of the wall damping function,  $f_\mu$ , from the experimental data of Patel, et al. ( $\square$ ), calculated from the HHL data, Eq. 19 with  $C_\mu = 0.115$ , ( $\circ$ ), and from the modified van Driest model, Eq. 20, with  $y_0^+ = 8$  and  $f_0 = 0.04$ , ( $+$ ).

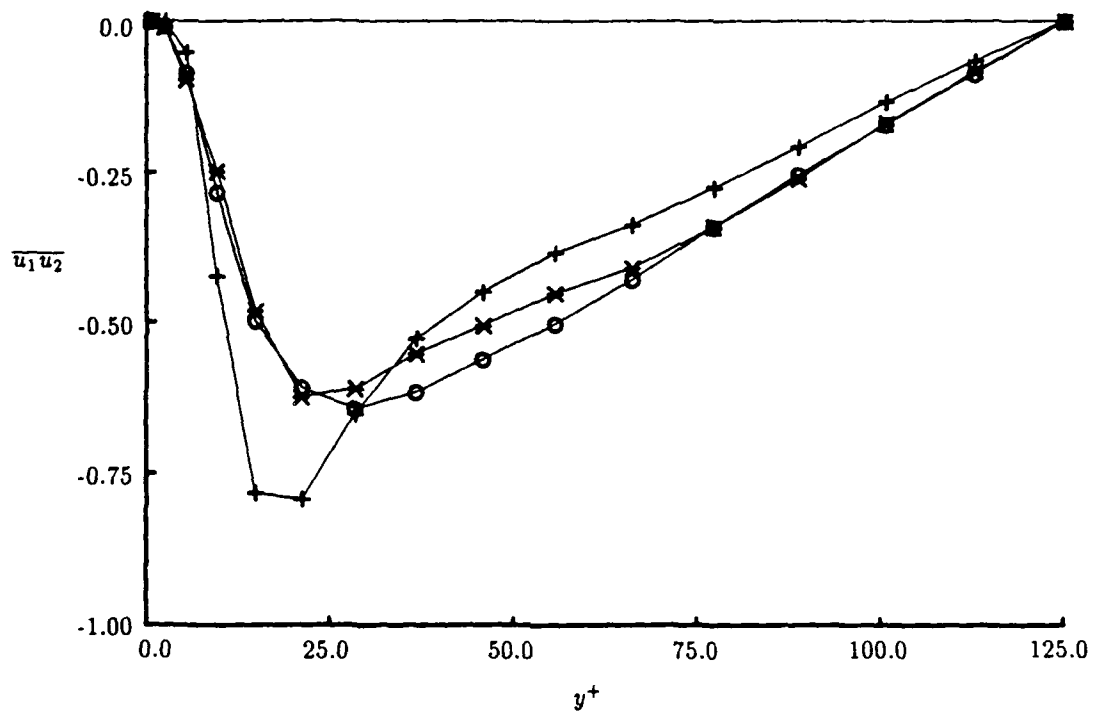


Fig. 14 — Comparison of Reynolds shear stress,  $\overline{u_1 u_2}$ , calculated from the HHL data (○), modeled using the modified van Driest wall damping model, Eq. 20, with  $f_0 = 0.04$ ,  $y_0^+ = 8$  and  $C_\mu = 0.115$ , (\*), and modeled with the standard van Driest wall damping model, Eq. 17, with  $C_\mu = 0.09$ , (+).

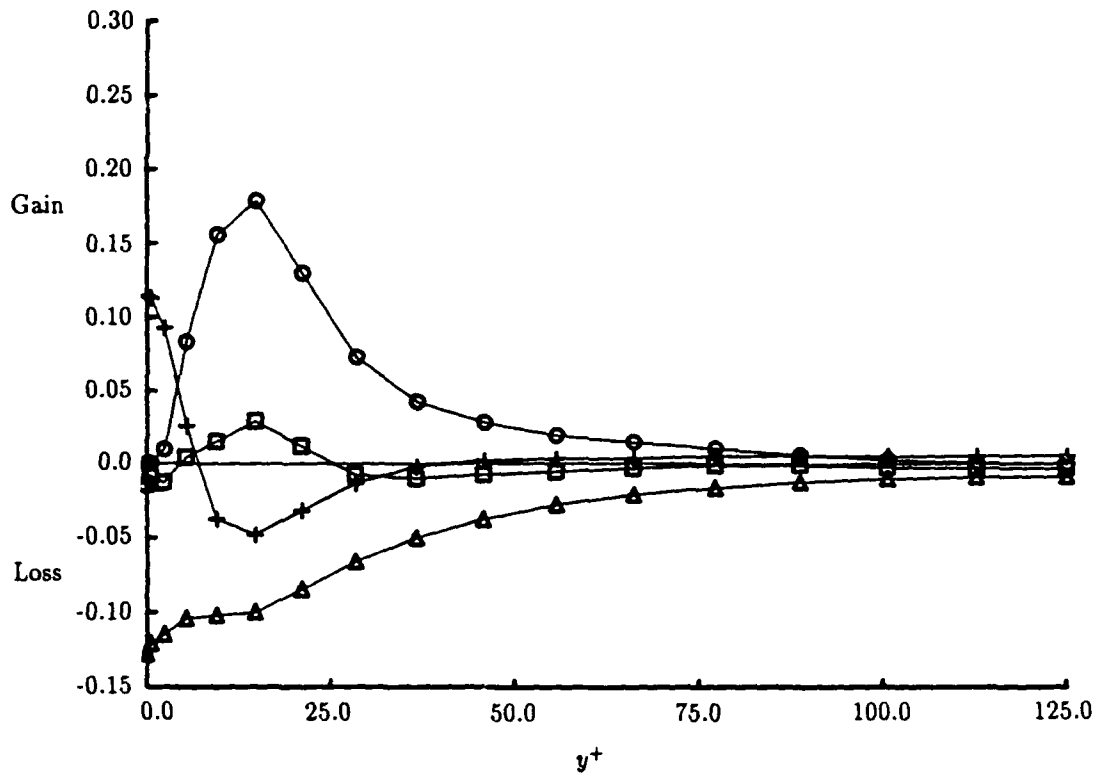


Fig. 15 — Budgets of the terms in the modeled transport equation for turbulence kinetic energy using the modified van Driest wall damping model, Eq. 20, with  $f_0 = 0.04$ ,  $y_0^+ = 8$  and  $C_\mu = 0.115$ . Dissipation term,  $\epsilon$ , ( $\Delta$ ); diffusion term (first term in Eq. 13) (+); production term,  $P$ , ( $\circ$ ); and sum of terms ( $\square$ ).

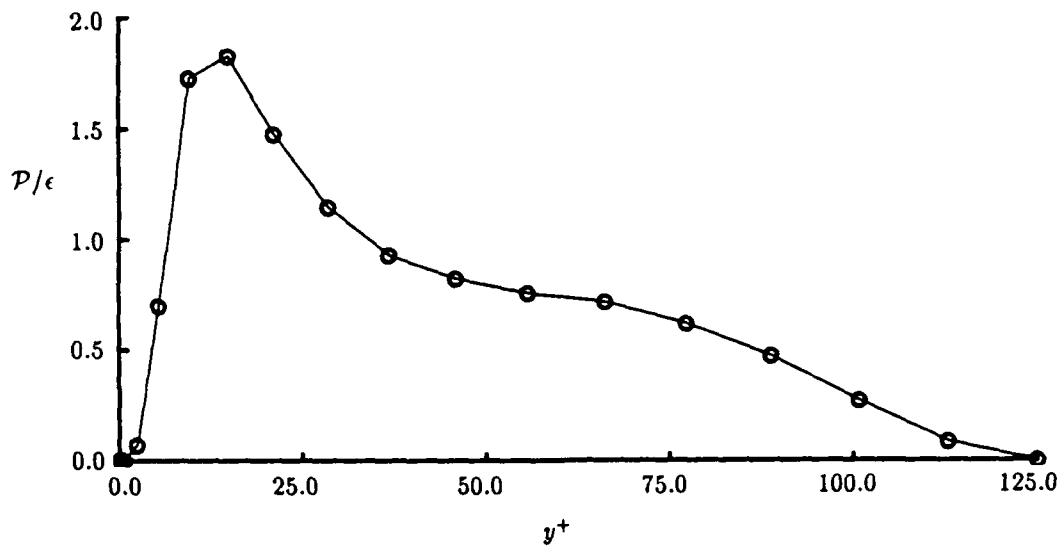


Fig. 16 — The distribution across the channel of the ratio of the production of turbulence kinetic energy,  $P$ , to the dissipation rate,  $\epsilon$ , as calculated from the direct simulation data.

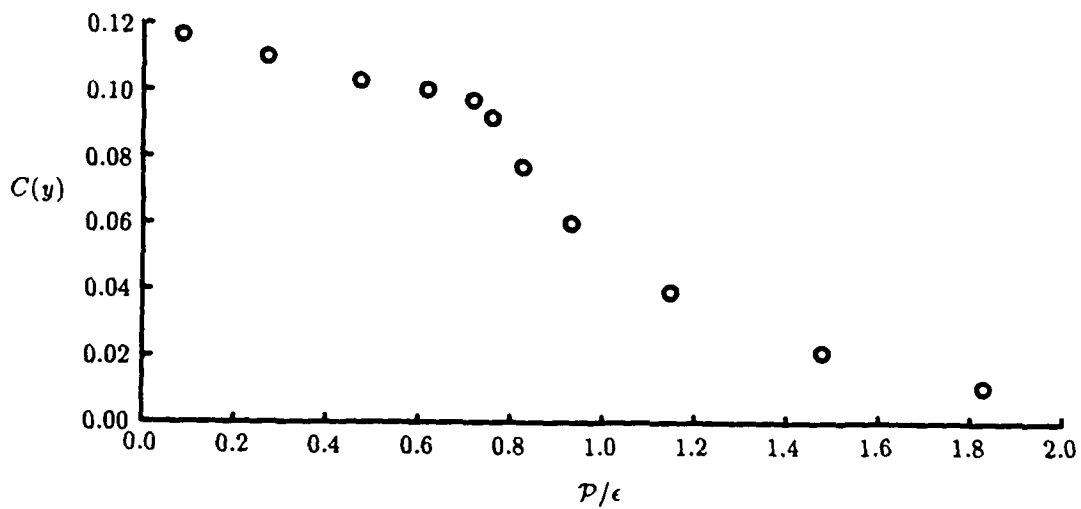


Fig. 17 — The eddy viscosity coefficient,  $C(y)$ , as a function of the ratio of the production of turbulence kinetic energy,  $P$ , to the dissipation rate,  $\epsilon$ .